PKC-mediated phosphorylation of nuclear lamins at a single serine residue regulates interphase nuclear size in *Xenopus* and mammalian cells

Lisa J. Edens, Matthew R. Dilsaver, and Daniel L. Levy*
Department of Molecular Biology, University of Wyoming, Laramie, WY 82071

ABSTRACT **How nuclear size is regulated is a fundamental cell-biological question with relevance to cancers, which often exhibit enlarged nuclei. We previously reported that conventional protein kinase C (cPKC) contributes to nuclear size reductions that occur during early *Xenopus* development. Here we report that PKC-mediated phosphorylation of lamin B3 (LB3) contributes to this mechanism of nuclear size regulation. By mapping PKC phosphorylation sites on LB3 and testing the effects of phosphomutants in *Xenopus laevis* embryos, we identify the novel site S267 as being an important determinant of nuclear size. Furthermore, FRAP studies demonstrate that phosphorylation at this site increases lamina dynamics, providing a mechanistic explanation for how PKC activity influences nuclear size. We subsequently map this *X. laevis* LB3 phosphorylation site to a conserved site in mammalian lamin A (LA), S268. Manipulating PKC activity in cultured mammalian cells alters nuclear size, as does expression of LA-S268 phosphomutants. Taken together, these data demonstrate that PKC-mediated lamin phosphorylation is a conserved mechanism of nuclear size regulation.**

Monitoring Editor
Karsten Weis
ETH Zurich

Received: Nov 16, 2016
Revised: Mar 15, 2017
Accepted: Mar 21, 2017

INTRODUCTION

Nuclear size varies in different cell types and during cell differentiation and development (Conklin, 1912; Wilson, 1925; Edens *et al.*, 2013; Borsos and Torres-Padilla, 2016), and nuclear size is often inappropriately enlarged in cancer (Zink *et al.*, 2004; Jevtic and Levy, 2014). It is largely unknown whether nuclear size directly affects cell function, motivating our studies on mechanisms of nuclear size regulation. Early *Xenopus laevis* development is a robust system in which to study nuclear size, as the early embryo undergoes a series of rapid cell divisions accompanied by reductions in both cell and nuclear size. After 12 cleavage cell cycles, the embryo reaches the midblastula transition (MBT), or stage 8, at which time zygotic transcription is up-regulated and cell divisions slow and become asynchronous (Nieuwkoop and Faber, 1967; Newport and Kirschner, 1982). From fertilization to the MBT, average nuclear volume decreases approximately fivefold, driven at least in part by reduced nuclear import kinetics and levels of cytoplasmic importin α. Nuclear size continues to scale smaller in post-MBT embryos, with a greater-than-threefold reduction in nuclear volume between stages 8 and 12. Furthermore, whereas pre-MBT nuclei continuously expand during brief 15- to 20-min interphase periods, nuclei in post-MBT embryos reach a steady-state size (Gerhart, 1980; Levy and Heald, 2010; Jevtic and Levy, 2015).

We previously reported an in vitro nuclear resizing assay in which large nuclei assembled de novo in *X. laevis* egg extract become smaller when incubated in cytoplasm isolated from stage 12 post-MBT *X. laevis* embryos (i.e., late-embryo extract). We showed that this nuclear shrinking depends on conventional protein kinase C (cPKC), a kinase family that includes PKC α and β and depends on diacyglycerol and calcium for activity (Newton, 2003). Furthermore, we showed that developmental reductions in nuclear size correlate with increased cPKC nuclear localization and activity, and manipulating cPKC activity in live *X. laevis* embryos led to concomitant changes in nuclear size within interphase. Taken together, these results implicated cPKC as a key regulator of nuclear size in post-MBT embryos (Edens and Levy, 2014a, 2016). An important question resulting from this earlier work was the identity of the cPKC substrates that control nuclear size.

This article was published online ahead of print in MBoC in Press (http://www.molbiolcell.org/cgi/doi/10.1091/mbc.E16-11-0786) on March 29, 2017.
The authors declare no competing financial interests.
*Address correspondence to: Daniel L. Levy (dlevy1@uwyo.edu).
Abbreviations used: cPKC, conventional protein kinase C; LA, lamin A; LB3, lamin B3; MBT, midblastula transition; NE, nuclear envelope; NPC, nuclear pore complex; PMA, phorbol 12-myristate 13-acetate.

Nuclear lamins—intermediate filament proteins that form a meshwork on the nucleoplasmic face of the nuclear envelope (NE)—are known PKC substrates (Simon and Wilson, 2013). During open mitosis, NE disassembly requires dissolution of the nuclear lamina, mediated by lamin phosphorylation by PKC and cyclin-dependent kinases (Heald and McKeon, 1990; Mall *et al*., 2012). Compared to global NE PKC activity at mitosis, localized PKC-mediated phosphorylation of the nuclear lamina is required for nuclear egress of certain viruses and large messenger ribonucleoprotein (mRNP) particles (Muranyi *et al*., 2002; Reynolds *et al*., 2004; Park and Baines, 2006; Speese *et al*., 2012; Hatch and Hetzer, 2014). In our nuclear shrinking assay, we observed PKC-dependent NE removal of lamin B3 (LB3), the primary lamin isoform found in *X. laevis* eggs and early embryos (Stick and Hausen, 1985), prompting us to test the hypothesis that nuclear size is regulated by direct cPKC-mediated phosphorylation of nuclear lamins.

In this study, we identify a novel cPKC phosphorylation site in LB3 that influences both nuclear lamina dynamics and nuclear size in *X. laevis* embryos and extracts. Furthermore, we show that cPKC activity affects nuclear size in several cultured mammalian cell lines. Finally, we demonstrate that the phosphorylation site identified in *Xenopus* LB3 is conserved in human lamin A (LA) and that phosphorylation at this site influences the association of LA with the NE and nuclear size. We propose that cPKC-mediated phosphorylation of nuclear lamins represents a conserved mechanism of nuclear size regulation by which lamin association with the NE is decreased by interphase phosphorylation, resulting in concomitant reductions in nuclear size.

RESULTS AND DISCUSSION

A single PKC phosphorylation site in lamin B3 influences *Xenopus* nuclear size

We previously demonstrated that nuclei assembled in *X. laevis* egg extract become smaller when incubated in cytoplasm isolated from stage 12 embryos (Figure 1A). This PKC-dependent nuclear shrinking is accompanied by an approximately fivefold increase in cPKC nuclear staining (Edens and Levy, 2014a). To determine whether PKC is acting within the nucleus to affect nuclear size, we performed the nuclear shrinking assay in the presence of wheat germ agglutinin (WGA), which binds glycosylated FG-nucleoporins at the nuclear pore complex (NPC), thereby blocking nucleocytoplasmic transport. In the presence of WGA, nuclei failed to shrink and nuclear cPKC staining was significantly reduced (Supplemental Figure S1), indicating that the target of cPKC is intranuclear. Having previously demonstrated that nuclear shrinking is accompanied by PKC-dependent removal of nuclear lamins (Edens and Levy, 2014a), we next tested whether PKC directly phosphorylates nuclear lamins to effect changes in nuclear size.

We incubated recombinant green fluorescent protein (GFP)-LB3 with purified cPKC protein or late-embryo extract and resolved the reisolated GFP-LB3 on a gel that maximizes phosphorylation-induced band shifts. A fraction of both the late embryo extract–treated and cPKC-treated GFP–LB3 protein exhibited reduced gel mobility (Figure 1B and Supplemental Figure S2A). To identify sites directly phosphorylated by cPKC, we subjected the LB3 samples treated with recombinant cPKC protein to phosphorylation-site mapping by mass spectrometry. Although several putative phosphorylation sites were identified (Figure 1C and Supplemental Figure S2B), two sites had the highest Ascores and could be unequivocally assigned (Beausoleil *et al*., 2006), representing likely authentic PKC phosphorylation sites. We were particularly interested in these two sites because they appeared to be novel, having not been previously identified in studies of mitotic lamin PKC phosphorylation (Simon and Wilson, 2013), with Thr-223 found in the second linker region and Ser-267 found in the 2B coil-coiled region (Figure 1D).

To test whether these phosphorylation sites influence nuclear size, we generated LB3 phospho-null alanine mutants. Single-cell *X. laevis* embryos were comicroinjected with morpholinos to reduce endogenous LB3 levels (Supplemental Figure S3, A–D) and mRNA encoding GFP-LB3 wild-type (wt), LB3-S267A, or LB3-T223A and allowed to develop to stage 12 (Figure 1E). We previously demonstrated that the GFP tag does not interfere with the nuclear localization of LB3 or its concentration-dependent effect on nuclear size (Jevtic *et al*., 2015). Embryos expressing the LB3-S267A mutant exhibited significantly larger nuclei than the LB3-wt– or LB3-T223A–microinjected embryos (Figure 1F), and no developmental defects were observed. Measurements of nuclear GFP-LB3 intensity showed that LB3-wt, LB3-S267A, and LB3-T223A were present at similar levels within nuclei (Supplemental Figure S3E), demonstrating that the nuclear import efficiency of the phospho-null mutants was not affected. We next treated the LB3-wt– and LB3-S267A–microinjected embryos with phorbol 12-myristate 13-acetate (PMA), a PKC activator. PMA treatment reduced nuclear size in LB3-wt–microinjected embryos to a greater extent than in embryos expressing LB3-S267A (Figure 1G), supporting the idea that S267 is normally phosphorylated by PKC. The fact that PMA still reduced nuclear size, albeit to a lesser extent, in LB3-S267A–expressing embryos might be explained by incomplete morpholino knockdown of endogenous LB3 and/or the presence of additional LB3 PKC phosphorylation sites or PKC substrates relevant to nuclear size control. Consistent with the phosphorylation status of S267 influencing nuclear size, microinjection of the phosphomimetic mutant GFP-LB3-S267E resulted in smaller nuclei (Figure 1H). Taken together, these data indicate that PKC-mediated phosphorylation of LB3 at S267 contributes to the regulation of nuclear size during early *X. laevis* development.

Lamin B3 mobility is increased by PKC phosphorylation

Having demonstrated that phosphorylation of LB3 by cPKC influences nuclear size, we next asked whether the mechanism of action was by altering the dynamic association of LB3 with the nuclear lamina. We assembled nuclei in *X. laevis* egg extract supplemented with GFP-LB3 and resuspended isolated nuclei in late-embryo extract. To quantify GFP-LB3 dynamics, we performed confocal fluorescence recovery after photobleaching (FRAP) on the surface of nuclei and quantified the recovery of GFP-LB3 signal into the bleached spot (Figure 2, A and B, and Supplemental Videos S1–S3). We chose to monitor LB3 dynamics in *Xenopus* extract rather than in embryos because time-lapse imaging in stage 12 embryos is complicated by rapid cell and nuclear movements and small nuclear size (Edens and Levy, 2014a). Consistent with previous nuclear lamin FRAP studies (Moir *et al*., 2000; Zaremba-Czogalla *et al*., 2012; Buxboim *et al*., 2014; Kochin *et al*., 2014), we observed that the association of LB3 with the NE was not very dynamic, exhibiting a mobile fraction of 16%. Nonetheless, inhibiting PKC activity with the small molecule chelerythrine significantly reduced the LB3 mobile fraction to <10%, comparable to that observed when nuclei were treated with heat-inactivated late-embryo extract (Figure 2C). It was also evident that spreading of photobleached GFP-LB3 throughout the NE was greatest for nuclei treated with late-embryo extract, consistent with LB3 being more dynamic in the presence of active PKC (Figure 2A).

We also examined the dynamics of the LB3-S267 phosphomutant proteins using the same FRAP assay. We found that LB3-S267A

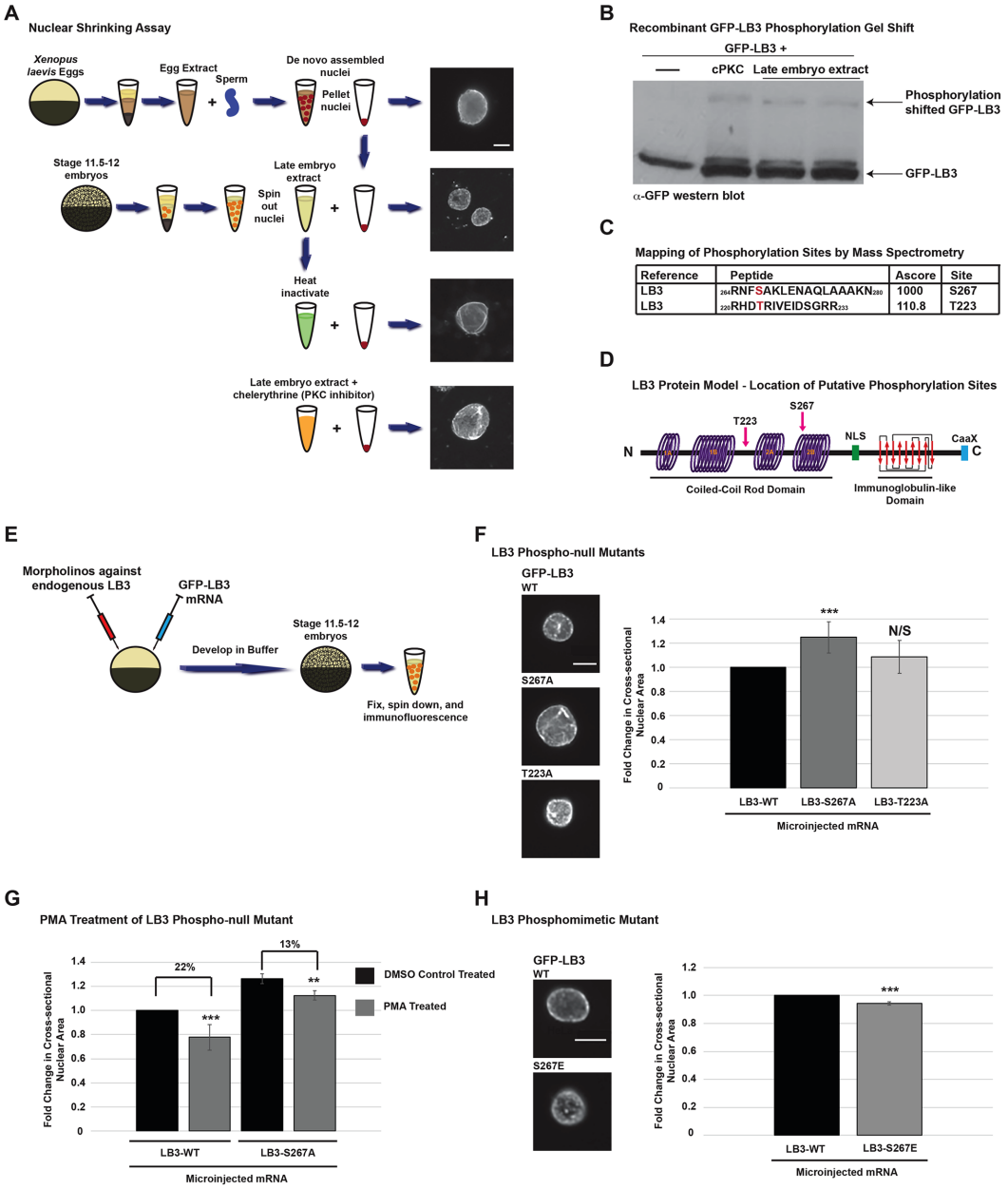

FIGURE 1: PKC-mediated phosphorylation of lamin B3 at S267 affects nuclear size in *X. laevis* embryos. (A) Schematic of the nuclear shrinking assay. Nuclei assembled in *X. laevis* egg extract are isolated by centrifugation and resuspended in cytoplasm derived from stage 11.5–12 *X. laevis* embryos (i.e., late-embryo extract). Nuclei incubated in late-embryo extract become smaller, whereas heat treatment of the extract or addition of the PKC inhibitor chelerythrine prevents nuclear shrinking. Nuclei were visualized by NPC staining (mAb414). Complete details of the nuclear shrinking assay are described elsewhere (Edens and Levy, 2014a, 2016). (B) Recombinant GFP-lamin B3 (GFP-LB3) was incubated with recombinant cPKC (Promega PepTag Non-Radioactive PKC Assay Kit) or two different late-embryo extracts for 30 min at 30°C. GFP-LB3 was isolated from the reactions using Ni-NTA beads (Qiagen), resolved on a SuperSep Phos-tag gel (Wako), and probed by Western blot using an anti-GFP antibody. (C) The shifted band from the cPKC reaction in B was excised from a Coomassie-stained gel (Supplemental Figure S2A) and subjected to phosphorylation-site mapping by mass spectrometry. The two sites with the highest Ascore values are shown in red, and complete results are in Supplemental Figure S2B. (D) The two putative phosphorylation sites identified in C are shown mapped onto the structural domains of LB3. (E–H) One-cell-stage *X. laevis* embryos were comicroinjected with morpholinos to knock down endogenous LB3 levels and equivalent amounts of mRNA (500 pg per embryo) expressing GFP-LB3 phosphorylation-site mutants. Stage 11.5–12 nuclei were isolated and quantified. For each sample, the cross-sectional nuclear areas of >160 nuclei were quantified, averaged, and normalized to LB3-wt (set at 1.0). (F) Cumulative LB3 phospho-null mutant data for three different fertilizations each with a minimum of 20 embryos. (G) Embryos microinjected as in F were treated with 6 nM PMA or DMSO for 90 min at room temperature before quantification. Cumulative data are shown for two different fertilizations each with a minimum of 25 embryos. (H) Cumulative LB3 phosphomimetic mutant data for two different fertilizations each with a minimum of 20 embryos. Bars, 10 μm. ***$p < 0.005$; **$p < 0.01$; N/S, not significant. Errors bars represent SD.

exhibited reduced mobility relative to wt (Figure 2D), consistent with phosphorylation at this site being important for increased LB3 mobility. The LB3-S267E mutant exhibited a similar mobile fraction to wt, suggesting that a significant fraction of LB3-wt molecules are normally phosphorylated at this site. Whereas PKC inhibition with chelerythrine reduced LB3-wt mobility to a nominal level, LB3-S267E mobility was unaffected by PKC inhibition (Figure 2D), strongly indicating that S267 phosphorylation is a primary determinant of PKC-dependent LB3 mobility. These data support a model by which PKC-dependent LB3-S267 phosphorylation modulates nuclear lamina dynamics, thereby affecting nuclear size.

PKC-dependent nuclear size control is conserved in mammalian cell culture

To determine whether cPKC-dependent nuclear size regulation is conserved outside of *Xenopus*, we investigated three cultured mammalian cell lines: HeLa (human cervical cancer cells), Ptk2 (rat-kangaroo epithelial kidney cells), and MRC-5 (human fetal lung fibroblasts). Nearly confluent cell monolayers were treated for 90 min with a PKC activator (PMA) or a cPKC inhibitor (Gö 6976). Consistent with our *Xenopus* findings, PMA treatment resulted in significantly smaller nuclei in all three cell lines. However, PKC inhibition increased nuclear size only in HeLa cells, perhaps because these cells are cancer derived and more

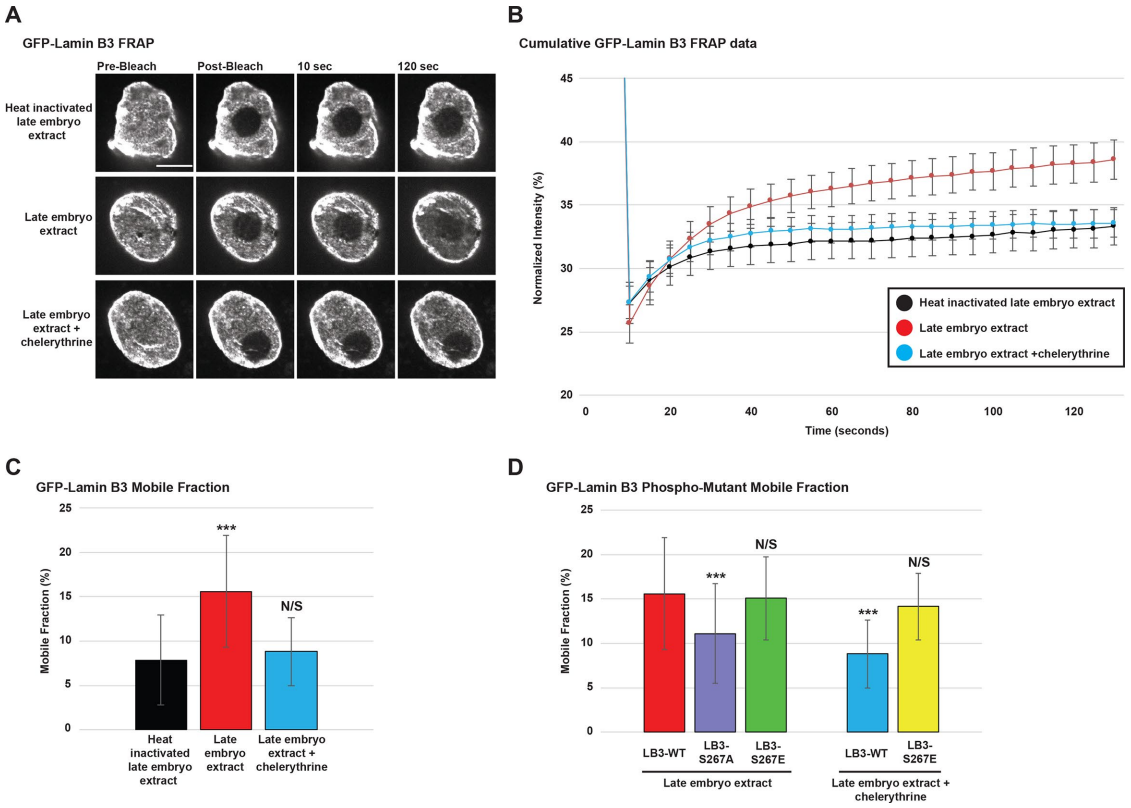

FIGURE 2: FRAP analysis of lamin B3 dynamics. (A) Nuclei were assembled in *X. laevis* egg extract at room temperature. At 30–40 min after initiating nuclear assembly, reactions were supplemented with 28 nM GFP-LB3. After an additional 60-min incubation, nuclei were isolated and resuspended in late-embryo extract as in Figure 1A. Where indicated, heat-inactivated late-embryo extract or late-embryo extract supplemented with 0.4 mM chelerythrine to inhibit PKC activity was used. Reactions were supplemented with an oxygen-scavenging mix. GFP-LB3 was imaged by confocal microscopy, and a 3.6-µm-radius circular spot on the surface of the nucleus was photobleached. After photobleaching, GFP-LB3 fluorescence recovery was detected by imaging every 5 s for a total of 120 s. Images from representative time lapses are shown (also see Supplemental Videos S1–S3). Bar, 10 µm. (B) For each FRAP time-lapse experiment, the mean GFP-LB3 fluorescence intensity of the photobleached region, entire nucleus, and a background region was measured at each time point. These data were analyzed using the easyFRAP application (Rapsomaniki *et al.*, 2012) and subjected to double normalization. The first postbleach image was acquired at 10 s, and prebleach intensities were normalized to 100%. Five independent experiments were performed, and time lapses were acquired for 46 late-embryo extract nuclei, 48 heat-inactivated late-embryo extract nuclei, and 44 late-embryo extract plus chelerythrine nuclei. The mean normalized GFP-LB3 fluorescence intensity within the bleached regions and SEM are shown for each time point. (C, D) For each acquired time lapse, normalized GFP-LB3 fluorescence intensity measurements within the bleached region were fitted to a single exponential that was used to estimate the mobile fraction with easyFRAP (Rapsomaniki *et al.*, 2012). The LB3-wt data with and without chelerythrine shown in D are the same data presented in C. In D, nuclei were assembled in *X. laevis* egg extract supplemented with the indicated GFP-LB3 phosphorylation-site mutants and then subjected to the nuclear shrinking assay and FRAP. We quantified 53 LB3-S267A, 55 LB3-S267E, and 33 LB3-S267E plus chelerythrine nuclei in four independent experiments. Note that estimated $t_{1/2}$ recovery times generally supported our conclusions about wt and mutant LB3 dynamics; however, low mobile fractions prevent accurate determination of $t_{1/2}$ values and so those data are not included. ***$p < 0.001$; N/S, not significant. Error bars represent SD.

amenable to nuclear size alterations (Figure 3A). The fact that we observed nuclear size changes after brief treatments with PMA or Gö 6976 indicates that these changes occurred within interphase and were not caused by postmitotic effects on nuclear size.

To explore further the effect of specific cPKC isoforms on nuclear size, we performed transient transfections with plasmids expressing constitutively active forms of PKC α and β (Supplemental Figure S4A). Expression of constitutively active PKC βII significantly reduced cross-sectional nuclear area in HeLa, Ptk2, and MRC-5 cells

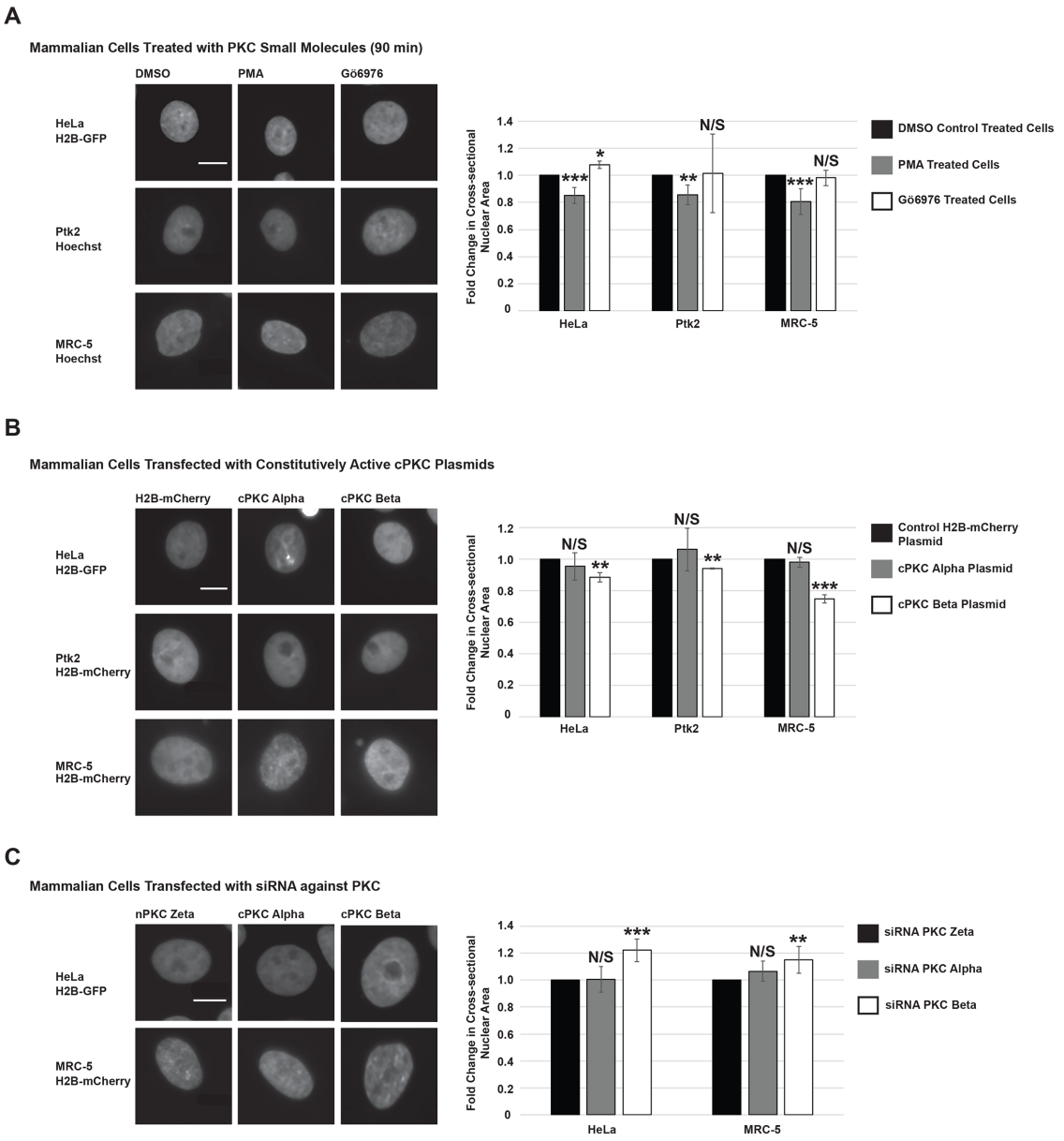

FIGURE 3: Altering PKC activity in cultured mammalian cells influences nuclear size. Representative images for the cell lines, with visualization methods indicated to the left. HeLa cells stably express H2B-GFP, whereas the Ptk2 and MRC-5 nuclei were visualized either with Hoechst or H2B-mCherry introduced by cotransfection. Cross-sectional nuclear area was quantified for >150 nuclei per sample, averaged, and normalized to the relevant control (set at 1.0). (A) Nearly confluent cells grown on glass coverslips were treated with a PKC activator (6 nM PMA) or cPKC inhibitor (2 μm Gö 6976; inhibits PKC α and β) for 90 min. Cumulative data from four independent experiments. Gö 6976 was used for these experiments rather than chelerythrine, which is known to disrupt cell adhesion (Zimmerman *et al.*, 2004; Tan *et al.*, 2011). (B) Cells were transiently cotransfected with plasmids expressing constitutively active cPKC α or βII and H2B-mCherry. Cells were fixed and imaged, using H2B-mCherry fluorescence to identify transfected cells. Cumulative data from three independent experiments. (C) Cells were transiently cotransfected with siRNA against the indicated PKC isoforms and a plasmid expressing H2B-mCherry. Cells were fixed and imaged, using H2B-mCherry fluorescence to identify transfected cells. The PKC ζ isoform was used as a negative control, as its expression is exclusively neuronal. Cumulative data from three independent experiments. These siRNA oligos designed against human PKC sequences were ineffective in Ptk2 rat-kangaroo cells. Bars, 10 μm. ***$p < 0.005$; **$p < 0.01$; *$p < 0.05$; N/S, not significant. Errors bars represent SD.

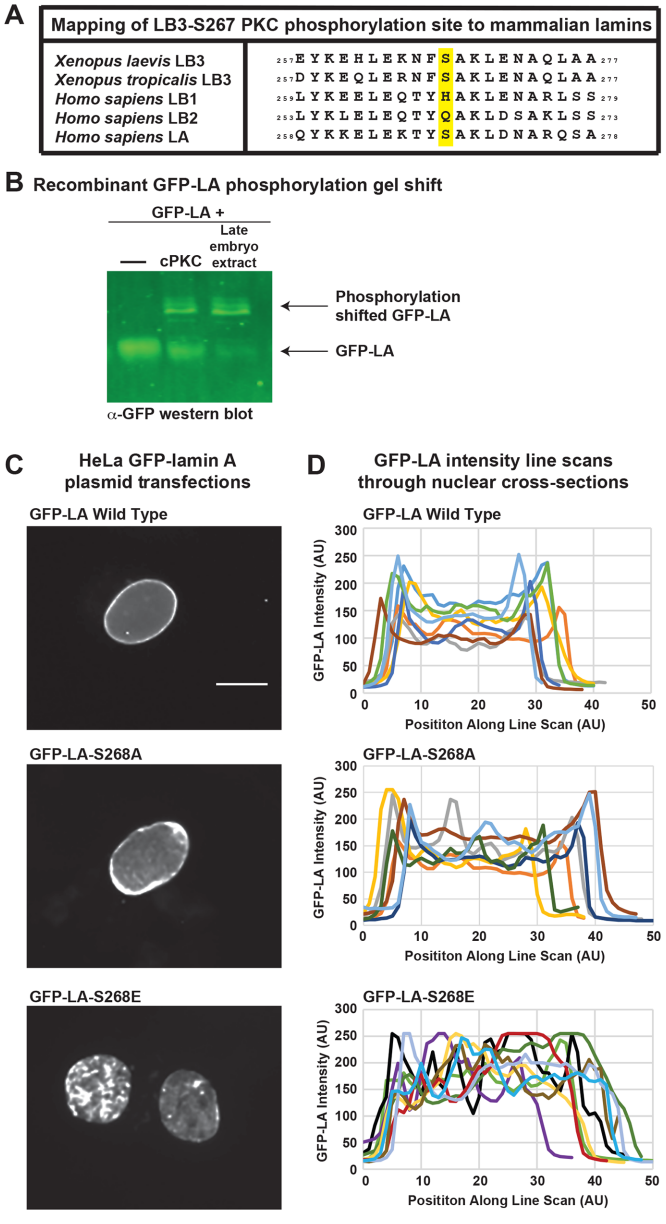

FIGURE 4: Nuclear distribution of human lamin A is altered by a conserved PKC phosphorylation site. (A) Protein sequence alignment of *Xenopus* and human nuclear lamins. The *Xenopus* LB3-S267 site is highlighted in yellow and shows conservation with S268 in human LA. (B) Experiments were performed as in Figure 1B, using recombinant human LA tagged with GFP (GFP-LA) as the substrate. (C) HeLa cells were transiently transfected with the indicated GFP-LA expression plasmids, and nuclei were visualized with GFP 2 d after transfection. Representative nuclei with similar total GFP-LA intensities. Bar, 10 μm. (D) Line scans measuring GFP-LA intensity through nuclear cross sections were acquired using ImageJ. Line scans for seven to nine representative nuclei are shown in each graph, with each trace representing one nucleus. For this analysis, cells with similar GFP-LA expression levels were selected based on nuclear GFP-LA intensity quantification (unpublished data). (E) For LA-wt and LA-S268A, GFP-LA intensity line scans, like those shown in D, exhibited clear peaks at the NE. The widths of these peaks were measured at the GFP-LA intensity corresponding to the nucleoplasmic signal for a given nucleus. The widths of both peaks were measured for 40 nuclei and averaged for a given sample. Cumulative data from four independent experiments. $^{**}p < 0.01$. Errors bars represent SD.

by up to 25% (Figure 3B). Conversely, knocking down PKC β levels by transient small interfering RNA (siRNA) transfection (Supplemental Figure S4B) increased cross-sectional nuclear area by up to 22% (Figure 3C). These results demonstrate that PKC β levels and activity influence nuclear size in mammalian cells to a greater extent than PKC α, consistent with *Xenopus* studies (Edens and Levy, 2014a). Taken together, these data suggest that cPKC represents a conserved mechanism of nuclear size regulation.

A conserved lamin A phosphorylation site influences lamin A nuclear distribution and nuclear size

Having demonstrated that cPKC influences nuclear size in mammalian cells, we next sought to determine whether the S267 phosphorylation site identified in *Xenopus* LB3 was conserved in mammalian lamins. Sequence alignments indicated that, although not found in B-type lamins, a conserved serine residue is present at S268 in lamin A (LA; Figure 4A). In addition, recombinant LA treated with cPKC or late-embryo extract exhibited a gel shift similar to that observed with LB3, indicating that LA is a substrate for PKC phosphorylation (Figure 4B). Note that A-type lamins are generally phosphorylated by PKC to mediate nuclear egress of viruses and large mRNP particles (Muranyi *et al.*, 2002; Reynolds *et al.*, 2004; Speese *et al.*, 2012).

To test the functional significance of the conserved serine residue in human LA, we generated LA phosphomutants. HeLa cells were transiently transfected with plasmids expressing GFP-LA-wt, LA-S268A, or LA-S268E (Supplemental Figure S4, C and D). The LA mutants exhibited striking differences in their nuclear distribution patterns (Figure 4C) regardless of whether endogenous LA levels were knocked down by siRNA (unpublished data). We observed enhanced NE localization of LA-S268A and the accumulation of LA-S268A plaques lining the NE. GFP-LA intensity line scans through representative nuclei (Figure 4D) revealed a nearly twofold increase in the GFP-LA NE peak widths for LA-S268A compared with wt (Figure 4E), suggesting a greater accumulation of the phospho-null LA mutant at the NE. In contrast, LA-S268E exhibited primarily nucleoplasmic puncta, with very little localization to the NE rim (Figure 4, C and D).

We previously reported that ectopic GFP-LA expression increases nuclear size in both HeLa and MRC-5 cells and that LA lacking the GFP tag has a similar effect (Jevtic *et al.*, 2015). In HeLa cells transiently cotransfected with siRNA against endogenous LA and plasmids expressing GFP-LA, we again noted a positive correlation between nuclear size and the level of LA expression, as quantified by nuclear GFP-LA intensity (Figure 5, A and B). Linear regression analysis suggested that LA-S268A expression increased nuclear size relative to LA-wt (Figure 5B), consistent with our *Xenopus* LB3-S267A findings (Figure 1F). To evaluate these data further and normalize for LA expression levels, we divided nuclei into bins based on their GFP-LA intensity. Across all but the highest GFP-LA–intensity bins, LA-S268A expression resulted in larger nuclei compared with LA-wt. The effect of LA-S268E on nuclear size varied, generally

exhibiting nuclear sizes intermediate between those of LA-wt and LA-S268A (Figure 5C). When nuclear sizes were averaged across multiple experiments irrespective of LA expression levels, both LA-S268A and LA-S268E expression resulted in nuclear cross-sectional areas ~20% larger than wt (Figure 5D). Of importance, the magnitude of nuclear size changes reported here is potentially physiologically relevant, falling within the clinical range of nuclear size increases in cancer cells (Wang *et al.*, 1992; Mossbacher *et al.*, 1996;

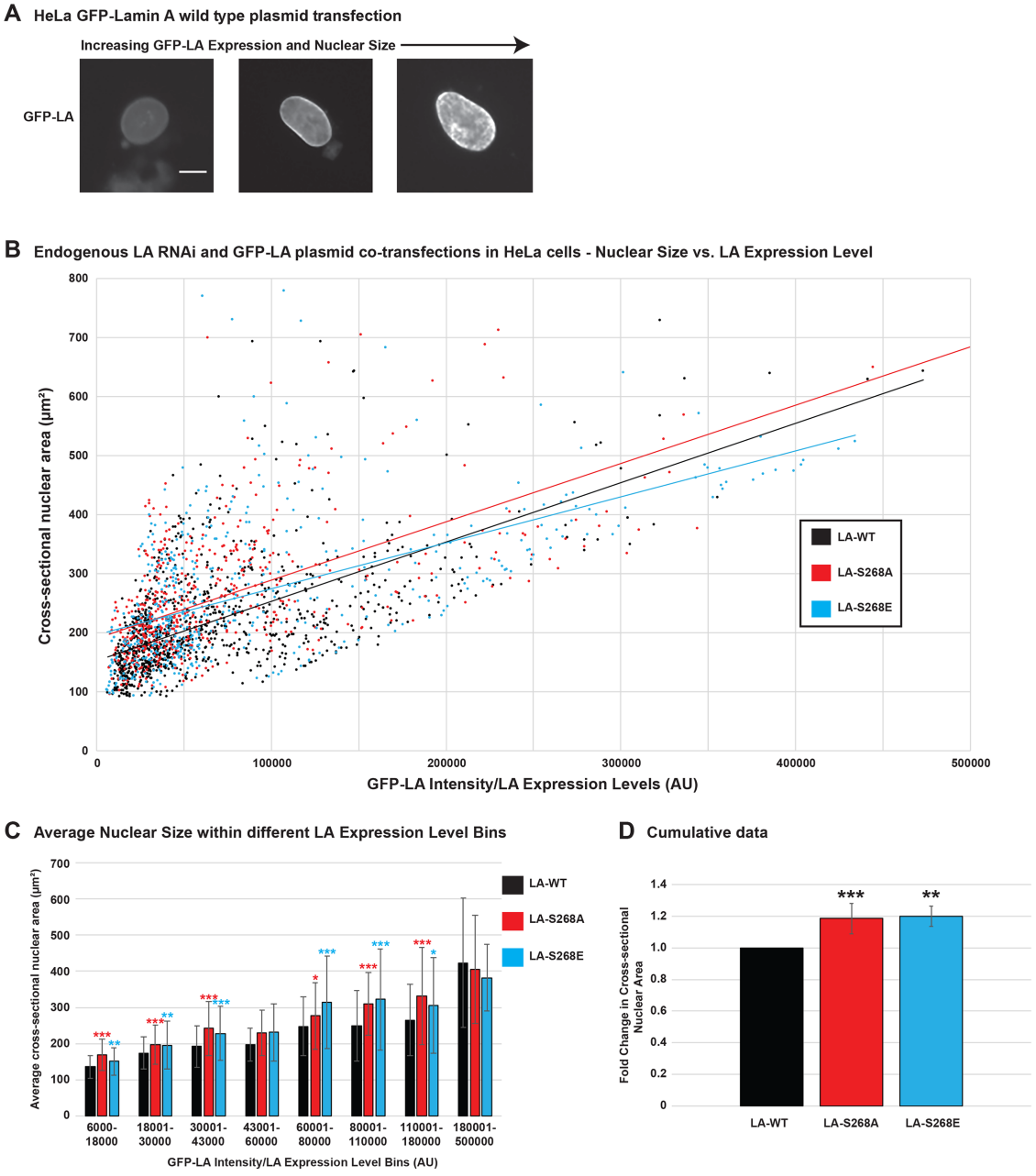

FIGURE 5: Phosphorylation of S268 on human lamin A influences nuclear size. HeLa cells were cotransfected with siRNA against endogenous LA and the indicated GFP-LA expression plasmids, and nuclei were visualized with GFP 2 d after transfection. The LA siRNA used here targets the 5′ UTR (Lund *et al.*, 2013), reduced endogenous LA expression levels by 81% (Supplemental Figure S4C), and does not target plasmid-expressed GFP-LA. (A) Increasing levels of LA-wt, as determined by GFP-LA intensity, correlate with increased nuclear size. Bar, 10 µm. (B) Cross-sectional nuclear area as a function of total nuclear GFP-LA intensity. Each data point represents one nucleus. Data from one representative experiment, including 1011 GFP-LA-wt nuclei, 585 GFP-LA-S268A nuclei, and 526 GFP-LA-S268E nuclei. Best-fit linear regression lines are plotted. (C) Nuclei were divided into bins based on GFP-LA intensity levels. Cumulative data from four independent experiments. Each bin includes a minimum of 100 nuclei per condition. Within each bin, Student's *t* tests were performed relative to LA-wt, and absence of asterisks indicates that the difference was not statistically significant. (D) Cumulative data from four independent experiments. More than 150 nuclei were quantified per condition and experiment, and nuclear size changes were normalized to LA-wt (set at 1.0). ***$p < 0.005$; **$p < 0.01$; *$p < 0.05$. Error bars represent SD.

Abdalla *et al.*, 2009; Vukovic *et al.*, 2016), as well as being sufficient to alter developmental timing in *Xenopus* embryos (Jevtic and Levy, 2015). Whereas PMA treatment reduced nuclear size in cells expressing LA-wt, nuclear size was refractory to PMA in cells expressing LA-S268A or LA-S268E (Supplemental Figure S4E), supporting the idea that S268 is a key PKC target in nuclear size regulation.

Although we have not demonstrated that S268 of LA is directly phosphorylated by PKC, this supposition is supported by 1) all of our experiments with the conserved serine residue in *Xenopus* lamin B3 (Figures 1 and 2), 2) observed effects of LA-S268 mutations on LA localization and nuclear size (Figures 4 and 5), and 3) our finding that activating PKC with PMA fails to reduce nuclear size in cells expressing LA-S268 mutants (Supplemental Figure S4E). Whereas our human LA and *Xenopus* LB3 results generally agreed with each other, one discrepancy concerned the phosphomimetic mutant—namely, LB3-S267E decreased nuclear size in *Xenopus* embryos, whereas LA-S268E increased HeLa nuclear size. This difference could be due to 1) the punctate nuclear localization of LA-S268E in HeLa cells potentially affecting mechanical properties of the nucleus (Lammerding *et al.*, 2006; Denais and Lammerding, 2014; Gruenbaum and Foisner, 2015; Zwerger *et al.*, 2015), 2) functional and structural differences between LB3 and LA, and/or 3) confounding effects of different B-type lamins being present in HeLa cells, whereas only one primary lamin protein is found in early *Xenopus* embryos (i.e., LB3). Note that at the highest LA expression levels, LA-S268E nuclei were smaller than wt (Figure 5C). Nonetheless, the novel lamin point mutants we describe here are, to the best of our knowledge, among the most precise and specific ways to manipulate nuclear size in cells and embryos. In the future, we anticipate that these mutants will be important tools in dissecting the functional significance of nuclear size with respect to chromatin organization and gene expression.

We show that PKC-mediated lamin phosphorylation is a conserved mechanism of nuclear size regulation. We propose that steady-state nuclear size is determined by a balance between nuclear import–mediated nuclear growth (Levy and Heald, 2010) and modulation of nuclear lamina dynamics by PKC activity and localization. The new results presented here have potentially important disease implications. An Emery–Dreifuss muscular dystrophy patient was identified with a LA-S268P mutation (Scharner *et al.*, 2011), and mutations in the adjacent amino acid, LA-Y267, are known to be pathogenic (Vytopil *et al.*, 2003; Carboni *et al.*, 2008). Cancer cells are often identified by their increased nuclear size (Zink *et al.*, 2004; Jevtic and Levy, 2014), and carcinogenesis is frequently associated with prognostic changes in lamin expression levels (Foster *et al.*, 2010; Chow *et al.*, 2012) and PKC signaling (Lonne *et al.*, 2010; Mochly-Rosen *et al.*, 2012; Urtreger *et al.*, 2012). In addition, altered PKC signaling and nuclear size have both been proposed as priming events in carcinogenesis (Prevostel *et al.*, 1997; Gokmen-Polar *et al.*, 2001; Chai and Brown, 2009). It is intriguing to speculate that the two might be causally related and that modulating the levels or activity of PKC and lamins might restore a normal nuclear size in some cancers, potentially abrogating features of the disease.

MATERIALS AND METHODS

Small molecules, plasmids, proteins, and siRNA

Small molecules. Chelerythrine chloride (C2932; Sigma-Aldrich), Gö 6976 (G1171; Sigma-Aldrich), and WGA (L9640; Sigma-Aldrich) were reconstituted in water. PMA (P8139; Sigma-Aldrich) was reconstituted in dimethyl sulfoxide (DMSO). For in vitro *Xenopus* experiments, chelerythrine was used at 0.4 mM. For *Xenopus* embryo and mammalian cell culture experiments, PMA was used at 6 nM and Gö 6976 at 2 μM.

Plasmids. We used mammalian expression vectors (pHACE) expressing constitutively active human PKC α (21233; Addgene) and mouse PKC βII (16383; Addgene). In each case, the N-terminal 29 amino acids encompassing the pseudosubstrate domain had been deleted (dNPS), giving rise to constitutive activity (Soh and Weinstein, 2003). Recombinant GFP-LB3 protein was expressed from GFP-LB3 pDEST17 (pDL5; Levy and Heald, 2010). Site-directed mutagenesis of pDL5 was performed to generate the S267A mutant (pDL58), T223A mutant (pDL60), and S267E mutant (pDL85). GFP-LB3 mRNA was synthesized from plasmid pCS2+ GFP-LB3 (pDL19; Levy and Heald, 2010). GFP-LB3-S267A was cloned from pDL58 into pCS2+ at *Bam*HI/*Xho*I (pDL71). GFP-LB3-T223A was cloned from pDL60 into pCS2+ at *Bam*HI/*Xho*I (pDL73). GFP-LB3-S267E was cloned from pDL85 into pCS2+ at *Bam*HI/*Xho*I (pDL86). Transfection of cultured mammalian cells was performed with GFP-lamin A pcDNA3.1 (pDL74; Jevtic *et al.*, 2015). Site-directed mutagenesis of pDL74 was performed to generate the S268A mutant (pDL83) and S268E mutant (pDL84). The H2B-mCherry mammalian expression vector was obtained from Anne Schlaitz (Zentrum für Molekulare Biologie der Universität Heidelberg).

Proteins. Recombinant GFP-lamin B3 (pDL5, pDL58, dDL85) and GFP-LA (pDL44) were expressed in bacteria and purified as previously described (Levy and Heald, 2010; Jevtic *et al.*, 2015).

siRNA sequences. To knock down expression of PKC, the following siRNAs were used: PKC ζ (SASI_Hs01_00116520; Sigma-Aldrich), PKC α (SASI_Hs01_00018815; Sigma-Aldrich), PKC β (SASI_Hs01_00071183; Sigma-Aldrich), and universal negative control (SIC001; Sigma-Aldrich). For LA knockdown, we used a DsiRNA (IDT): sense, 5′-GACUCCGAGCAGUCUCUGUCCUUCGAC-3′, and antisense, 5′-GUCGAAGGACAGAGACUGCUCGGAGUC-3′. This DsiRNA sequence is based on a previously described shRNA that targets the 5′ untranslated region (UTR) of the LA transcript (Lund *et al.*, 2013) and therefore does not target GFP-LA expressed from plasmids pDL74, pDL83, and pDL84.

Xenopus extracts and nuclear shrinking assay

All *Xenopus* procedures and studies were conducted in compliance with the U.S. Department of Health and Human Services Guide for the Care and Use of Laboratory Animals. Protocols were approved by the University of Wyoming Institutional Animal Care and Use Committee (Assurance #A-3216-01). The following procedures have been previously described (Edens and Levy, 2014a, 2016). *X. laevis* egg extracts and sperm nuclei were used to assemble nuclei in vitro. Reactions were supplemented with ~28 nM recombinant wt or mutant GFP-LB3 protein 45 min after initiating nuclear assembly. Egg extract nuclei were isolated and resuspended in late-embryo extract to induce nuclear shrinking. For immunofluorescence, nuclei in egg or embryo extract were fixed, spun onto coverslips, and processed for immunofluorescence. A primary rabbit antibody that recognizes phospho–PKC α/β (bs-3333R; Bioss USA) was used at a dilution of 1:100. For LB3 staining, we used a previously described rabbit LB3 antibody at 1:500 (Levy and Heald, 2010). For NPC staining, we used mAb414 (Covance) at 1:1000. Secondary antibodies were Alexa Fluor 488 or 568 anti-mouse or anti-rabbit immunoglobulin G (Molecular Probes) used at 1:1000.

In vitro PKC reactions and Western blots

In vitro phosphorylation of GFP-LB3 and GFP-LA was performed with the Promega PepTag Non-Radioactive PKC Assay kit (V5330). Reactions included 0.2 μM recombinant GFP-LB3 or GFP-LA, 10 ng

of recombinant PKC α/β, phosphatidylserine micelles, reaction buffer, and protease inhibitors in a final volume of 25 µl. In some cases where indicated, recombinant GFP-LB3 or GFP-LA was treated with 25 µl of late-embryo extract rather than recombinant PKC. Reactions were incubated at 30°C for 30 min before isolating GFP-LB3 or GFP-LA using Ni–nitrilotriacetic acid (NTA) resin (Qiagen) under denaturing conditions. Protein samples were supplemented with SDS–PAGE sample buffer, boiled for 5 min, and separated on a 10% SuperSep Phos-tag gel (Wako). For mapping of phosphorylation sites, the cPKC reaction was scaled up fourfold to 100 µl, gels were stained with Coomassie, and the lower-mobility GFP-LB3 band resulting from phosphorylation was excised. Western blots were performed as previously described (Edens and Levy, 2014a; Jevtic *et al*., 2015) with the following antibodies: rabbit anti-GFP antibody (A-6455; Invitrogen) used at 1:2000, mouse anti-actin antibody (AM1965b; Abgent) used at 1:200, rabbit pan-PKC antibody (sc-10800; Santa Cruz Biotechnology) used at 1:1000, and mouse Ran antibody used as previously described (Levy and Heald, 2010). *Xenopus* embryo or HeLa cell extracts were probed by Western blot using a rabbit antibody that specifically recognizes LB3 (R12-2960; Assay Biotech) at 1:500 or a mouse antibody against lamin A (MCA-4C4; EnCor Biotechnology) at 1:10,000, respectively. We verified that these lamin antibodies were unique for a given lamin type by testing them against recombinant lamin proteins (Jevtic *et al*., 2015). Secondary antibodies included a 1:15,000 dilution of goat anti-rabbit horseradish peroxidase (HRP; ImmunoPure Antibody 31460; Thermo Scientific) and 1:20,000 dilution of IRDye 800CW anti-rabbit (926-32211; Li-Cor) or IRDye 680RD anti-mouse (925-68070; Li-Cor). Detection was performed as previously described for HRP (Edens and Levy, 2014a) or infrared fluorescence (Jevtic *et al*., 2015). Band quantification was performed with ImageStudio.

Phosphorylation-site mapping

Phosphorylation-site mapping was performed by the Taplin Mass Spectrometry Facility (Cell Biology Department, Harvard Medical School, Boston, MA). Excised gel bands were cut into ~1 mm^3 pieces. The samples were reduced with 1 mM dithiothreitol for 30 min at 60°C and then alkylated with 5 mM iodoacetamide for 15 min in the dark at room temperature. Gel pieces were then subjected to a modified in-gel trypsin digestion procedure (Shevchenko *et al*., 1996). Gel pieces were washed and dehydrated with acetonitrile for 10 min, followed by removal of acetonitrile. Pieces were then completely dried in a SpeedVac. Rehydration of the gel pieces was with 50 mM ammonium bicarbonate solution containing 12.5 ng/µl modified sequencing-grade trypsin (Promega, Madison, WI) at 4°C. Samples were then placed in a 37°C room overnight. Peptides were later extracted by removing the ammonium bicarbonate solution, followed by one wash with a solution containing 50% acetonitrile and 1% formic acid. The extracts were then dried in a SpeedVac (~1 h) and stored at 4°C until analysis.

On the day of analysis, the samples were reconstituted in 5–10 µl of HPLC solvent A (2.5% acetonitrile, 0.1% formic acid). A nanoscale reverse-phase HPLC capillary column was created by packing 2.6-µm C18 spherical silica beads into a fused silica capillary (100-µm inner diameter by ~30-cm length) with a flame-drawn tip (Peng and Gygi, 2001). After equilibrating the column, each sample was loaded via a Famos autosampler (LC Packings, San Francisco, CA) onto the column. A gradient was formed, and peptides were eluted with increasing concentrations of solvent B (97.5% acetonitrile, 0.1% formic acid). As each peptide was eluted, it was subjected to electrospray ionization and then entered into an LTQ Orbitrap Velos Pro ion-trap mass spectrometer (Thermo Fisher Scientific, San Jose, CA). Eluting peptides were detected, isolated, and fragmented to produce a tandem mass spectrum of specific fragment ions for each peptide. Peptide sequences (and hence protein identity) were determined by matching protein or translated nucleotide databases with the acquired fragmentation pattern by the software program Sequest (ThermoFinnigan, San Jose, CA; Eng *et al*., 1994). The modification of 79.9663 mass units to serine, threonine, and tyrosine was included in the database searches to determine phosphopeptides. Phosphorylation assignments were determined by the Ascore algorithm (Beausoleil *et al*., 2006). All databases include a reversed version of all of the sequences, and the data were filtered to between a 1 and 2% peptide false discovery rate.

Xenopus embryo microinjections

X. laevis embryos were generated, dejellied, and microinjected as previously described (Jevtic and Levy, 2015). One-cell embryos were comicroinjected with a 10-nl mixture of 1 mM LB3 morpholino oligonucleotides (Gene Tools) and 50 ng/µl GFP-LB3 mRNA using a Picospritzer III and allowed to develop to stage 12. A mixture of two morpholinos was used to target both LB3 isoforms: 5′-GGCCATAGTTTCCCTGTGAGTCCA-3′ and 5′-CGTAGCCATATTGTCTCTGAGTCCC-3′. These oligos target the 5′ UTR of endogenous LB3 transcripts and not the microinjected GFP-LB3 mRNA. In some experiments, a standard negative control morpholino oligo was used: 5′-CCTCTTACCTCAGTTACAATTTATA-3′. To generate mRNA for microinjections, plasmids pDL19, pDL71, pDL73, and pDL86 were linearized with *Not*I, and mRNA was expressed from the SP6 promoter using the mMessage mMachine kit (Ambion). Embryo extract was prepared from 15–50 embryos, and nuclei were fixed, spun onto coverslips, and stained with Hoechst as previously described (Edens and Levy, 2014a). GFP-LB3 fluorescence was used to quantify nuclear size.

Microscopy and image quantification

Wide-field microscopy was performed with an Olympus BX51 fluorescence microscope using an Olympus UPlanFl 20×/0.50 Ph1 objective. Images were acquired with a QIClick Digital CCD Camera, Mono, 12-bit (model QIClick-F-M-12), at room temperature using Olympus cellSens software. Images for measuring fluorescence intensity were acquired using the same exposure times. Total fluorescence intensity and cross-sectional nuclear area were measured from the original thresholded images using MetaMorph software (Molecular Devices). For publication, images were cropped using ImageJ but were otherwise unaltered. We previously demonstrated that cross-sectional nuclear area serves as an accurate proxy for total nuclear surface area and volume (Edens and Levy, 2014a; Jevtic and Levy, 2015).

Where indicated, confocal imaging was performed on a spinning-disk confocal microscope based on an Olympus IX71 microscope stand equipped with a five-line LMM5 laser launch (Spectral Applied Research) and switchable two-fiber output to facilitate imaging through either a Yokogawa CSU-X1 spinning-disk head or total internal reflection fluorescence illuminator. Confocal images were acquired with an electron-multiplying charge-coupled device camera (ImagEM; Hamamatsu) using an Olympus APO N 60× O/1.49 numerical aperture objective. *Z*-axis focus was controlled using a Piezo Pi-Foc (Physik Instrumente), and multiposition imaging was achieved using a motorized Ludl stage. Image acquisition and all system components were controlled using MetaMorph software, and images for measuring fluorescence intensity were acquired using the same exposure times.

FRAP experiments

Nuclei were assembled in *X. laevis* egg extract at room temperature. At 30–40 min after initiating nuclear assembly, reactions were supplemented with ~28 nM GFP-LB3. After an additional 60-min incubation, nuclei were isolated and resuspended in late-embryo extract as depicted in Figure 1A. Where indicated, we used heat-inactivated late-embryo extract treated at 56°C for 30 min or late-embryo extract supplemented with ~0.4 mM chelerythrine to inhibit PKC activity. Specific details of this nuclear shrinking assay are given elsewhere (Edens and Levy, 2014b, 2016). Reactions were supplemented with an oxygen-scavenging mix to minimize photodamage (Aitken *et al.*, 2008) and sealed between a slide and coverslip using a Pap pen. Imaging of GFP-LB3 incorporated into nuclei was accomplished by spinning-disk confocal microscopy using an Olympus UPlanApo 60×/1.20W objective. The surface of the NE juxtaposed to the coverslip was brought into focus, and a 3.6-µm-radius circular spot on the surface of the nucleus was photobleached using an iLas2 system (BioVision Technologies) with a 54-ms pulse of a 405-nm laser set at 30% power. After photobleaching, GFP-LB3 FRAP was detected by imaging every 5 s for a total of 120 s. For each FRAP time-lapse experiment, ImageJ was used to measure mean GFP-LB3 fluorescence intensity of the photobleached region, entire nucleus, and a background region at each time point. These data were analyzed using the easyFRAP application (Rapsomaniki *et al.*, 2012), and subjected to double normalization. Prebleach intensities were normalized to 100%.

Mammalian cell culture

Cell lines used were MRC-5 normal human lung fibroblasts, HeLa cells with or without stable H2B-GFP expression, and Ptk2 rat-kangaroo epithelial kidney cells. All cell lines were cultured at 37°C with 5% CO_2 using DMEM for MRC-5 and HeLa-H2B-GFP cell lines, Eagle's minimum essential medium for the unlabeled HeLa cell line, and RPMI for Ptk2 cells. All media were supplemented with 10% fetal bovine serum and 50 IU/ml penicillin and streptomycin. For transient transfections, cells were grown in 24-well plates to 70–90% confluency. Transient plasmid transfections were performed with Lipofectamine 3000 (Invitrogen). Briefly, in one tube, 1.5 µg of DNA was added to 25 µl of Opti-MEM medium plus 3 µl of P3000 reagent. In a separate tube, 1.5 µl of Lipofectamine 3000 reagent was added to 25 µl of Opti-MEM media. The two were mixed and incubated at room temperature for 5 min. Medium was removed from the 24-well plates and replaced with 500 µl/well of fresh culture medium and 50 µl of DNA–Lipofectamine complex. At 6 h (HeLa), 12 h (Ptk2), or 48 h (MRC-5) after transfection, cells were seeded onto acid-washed 18-mm square coverslips in 35-mm^2 dishes with 2 ml of fresh culture medium. At 24 h later, coverslips were washed with phosphate-buffered saline (without Mg^{2+} and Ca^{2+}), fixed with 4% paraformaldehyde for 20 min, washed, stained with 5 µg/ml Hoechst for 5 min, washed, mounted in Vectashield (Vector Laboratories), and sealed with nail polish. Transient siRNA transfections were performed with Lipofectamine RNAiMAX (Invitrogen). Briefly, 3 µl of 10 µM siRNA was diluted in 50 µl of Opti-MEM medium, 3 µl of Lipofectamine RNAiMAX reagent was diluted in 50 µl of Opti-MEM, and the two were mixed and incubated at room temperature for 5 min. The 50-µl transfection mixture was added to 500 µl of culture medium and incubated for 1 d (HeLa) or 3 d (MRC-5). Where indicated and to identify transfected cells, cotransfections were performed with 1.5 µg of H2B-mCherry plasmid. Cells were then seeded onto coverslips, cultured an additional 24 h, and fixed and processed as described for plasmid transfections. For small-molecule treatment, cells were seeded onto acid-washed 18-mm-square coverslips in 35-mm^2 dishes with 2 ml of fresh culture medium. After 24 h, the medium was supplemented with PMA (6 nM) or Gö 6976 (2 µM). After a 90-min treatment, cells were fixed and processed as described for plasmid transfections. Images were acquired and nuclear sizes quantified as described under *Microscopy and image quantification*.

Statistics

Unless otherwise noted, nuclear cross-sectional areas were measured from thresholded images in MetaMorph (Molecular Devices). For each coverslip, at least 105, and usually >310, nuclei were quantified, and areas were averaged. Unless otherwise noted, nuclear area measurements were normalized to controls. Averaging and statistical analysis were performed for independently repeated experiments. Two-tailed Student's *t* tests assuming equal variances were performed in Excel (Microsoft) to evaluate statistical significance. The *p* values, number of independent experiments, and error bars are given in the figure legends.

ACKNOWLEDGMENTS

We thank members of the Levy lab, as well as our colleagues in the Department of Molecular Biology, for helpful advice and discussions; Jay Gatlin, Jason Gigley, and Anya Lyuksyutova for cultured mammalian cell lines; and Karen White for constructive comments on the manuscript. This work was supported by the National Institutes of Health/National Institute of General Medical Sciences (R01GM113028) and the American Cancer Society (RSG-15-035-01-DDC).

REFERENCES

Abdalla F, Boder J, Markus R, Hashmi H, Buhmeida A, Collan Y (2009). Correlation of nuclear morphometry of breast cancer in histological sections with clinicopathological features and prognosis. Anticancer Res 29, 1771–1776.

Aitken CE, Marshall RA, Puglisi JD (2008). An oxygen scavenging system for improvement of dye stability in single-molecule fluorescence experiments. Biophys J 94, 1826–1835.

Beausoleil SA, Villen J, Gerber SA, Rush J, Gygi SP (2006). A probability-based approach for high-throughput protein phosphorylation analysis and site localization. Nat Biotechnol 24, 1285–1292.

Borsos M, Torres-Padilla ME (2016). Building up the nucleus: nuclear organization in the establishment of totipotency and pluripotency during mammalian development. Genes Dev 30, 611–621.

Buxboim A, Swift J, Irianto J, Spinler KR, Dingal PC, Athirasala A, Kao YR, Cho S, Harada T, Shin JW, Discher DE (2014). Matrix elasticity regulates lamin-a,c phosphorylation and turnover with feedback to actomyosin. Curr Biol 24, 1909–1917.

Carboni N, Mura M, Marrosu G, Cocco E, Ahmad M, Solla E, Mateddu A, Maioli MA, Marini S, Nissardi V, *et al.* (2008). Muscle MRI findings in patients with an apparently exclusive cardiac phenotype due to a novel LMNA gene mutation. Neuromuscul Disord 18, 291–298.

Chai H, Brown RE (2009). Field effect in cancer—an update. Ann Clin Lab Sci 39, 331–337.

Chow KH, Factor RE, Ullman KS (2012). The nuclear envelope environment and its cancer connections. Nat Rev Cancer 12, 196–209.

Conklin E ((1912). Cell size and nuclear size. J Exp Embryol 12, 1–98.

Denais C, Lammerding J (2014). Nuclear mechanics in cancer. Adv Exp Med Biol 773, 435–470.

Edens LJ, Levy DL (2014a). cPKC regulates interphase nuclear size during Xenopus development. J Cell Biol 206, 473–483.

Edens LJ, Levy DL (2014b). Size scaling of subcellular organelles and structures in Xenopus laevis and Xenopus tropicalis. In: Xenopus Development, ed. M Kloc and JZ Kubiak, Hoboken, NJ: John Wiley & Sons, 325–345.

Edens LJ, Levy DL (2016). A cell-free assay using Xenopus laevis embryo extracts to study mechanisms of nuclear size regulation. J Vis Exp 114, 10.3791/54173.

Edens LJ, White KH, Jevtic P, Li X, Levy DL (2013). Nuclear size regulation: from single cells to development and disease. Trends Cell Biol 23, 151–159.

Eng JK, McCormack AL, Yates JR (1994). An approach to correlate tandem mass spectral data of peptides with amino acid sequences in a protein database. J Am Soc Mass Spectrom 5, 976–989.
Foster CR, Przyborski SA, Wilson RG, Hutchison CJ (2010). Lamins as cancer biomarkers. Biochem Soc Trans 38, 297–300.
Gerhart JC (1980). Mechanisms regulating pattern formation in the amphibian egg and early embryo. In: Biological Regulation and Development, Vol. 2, ed. RF Goldberger, New York: Plenum, 133–316.
Gokmen-Polar Y, Murray NR, Velasco MA, Gatalica Z, Fields AP (2001). Elevated protein kinase C betaII is an early promotive event in colon carcinogenesis. Cancer Res 61, 1375–1381.
Gruenbaum Y, Foisner R (2015). Lamins: nuclear intermediate filament proteins with fundamental functions in nuclear mechanics and genome regulation. Annu Rev Biochem 84, 131–164.
Hatch E, Hetzer M (2014). Breaching the nuclear envelope in development and disease. J Cell Biol 205, 133–141.
Heald R, McKeon F (1990). Mutations of phosphorylation sites in lamin A that prevent nuclear lamina disassembly in mitosis. Cell 61, 579–589.
Jevtic P, Edens LJ, Li X, Nguyen T, Chen P, Levy DL (2015). Concentration-dependent effects of nuclear lamins on nuclear size in Xenopus and mammalian cells. J Biol Chem 290, 27557–27571.
Jevtic P, Levy DL (2014). Mechanisms of nuclear size regulation in model systems and cancer. Adv Exp Med Biol 773, 537–569.
Jevtic P, Levy DL (2015). Nuclear size scaling during Xenopus early development contributes to midblastula transition timing. Curr Biol 25, 45–52.
Kochin V, Shimi T, Torvaldson E, Adam SA, Goldman A, Pack CG, Melo-Cardenas J, Imanishi SY, Goldman RD, Eriksson JE (2014). Interphase phosphorylation of lamin A. J Cell Sci 127, 2683–2696.
Lammerding J, Fong LG, Ji JY, Reue K, Stewart CL, Young SG, Lee RT (2006). Lamins A and C but not lamin B1 regulate nuclear mechanics. J Biol Chem 281, 25768–25780.
Levy DL, Heald R (2010). Nuclear size is regulated by importin alpha and Ntf2 in Xenopus. Cell 143, 288–298.
Lonne GK, Cornmark L, Zahirovic IO, Landberg G, Jirstrom K, Larsson C (2010). PKCalpha expression is a marker for breast cancer aggressiveness. Mol Cancer 9, 76.
Lund E, Oldenburg AR, Delbarre E, Freberg CT, Duband-Goulet I, Eskeland R, Buendia B, Collas P (2013). Lamin A/C-promoter interactions specify chromatin state-dependent transcription outcomes. Genome Res 23, 1580–1589.
Mall M, Walter T, Gorjanacz M, Davidson IF, Nga Ly-Hartig TB, Ellenberg J, Mattaj IW (2012). Mitotic lamin disassembly is triggered by lipid-mediated signaling. J Cell Biol 198, 981–990.
Mochly-Rosen D, Das K, Grimes KV (2012). Protein kinase C, an elusive therapeutic target? Nat Rev Drug Discov 11, 937–957.
Moir RD, Yoon M, Khuon S, Goldman RD (2000). Nuclear lamins A and B1: different pathways of assembly during nuclear envelope formation in living cells. J Cell Biol 151, 1155–1168.
Mossbacher U, Knollmayer S, Binder M, Steiner A, Wolff K, Pehamberger H (1996). Increased nuclear volume in metastasizing "thick" melanomas. J Invest Dermatol 106, 437–440.
Muranyi W, Haas J, Wagner M, Krohne G, Koszinowski UH (2002). Cytomegalovirus recruitment of cellular kinases to dissolve the nuclear lamina. Science 297, 854–857.
Newport J, Kirschner M (1982). A major developmental transition in early Xenopus embryos: I. Characterization and timing of cellular changes at the midblastula stage. Cell 30, 675–686.
Newton AC (2003). Regulation of the ABC kinases by phosphorylation: protein kinase C as a paradigm. Biochem J 370, 361–371.
Nieuwkoop PD, Faber J (1967). Normal Table of Xenopus laevis (Daudin), Amsterdam: North-Holland.
Park R, Baines JD (2006). Herpes simplex virus type 1 infection induces activation and recruitment of protein kinase C to the nuclear membrane and increased phosphorylation of lamin B. J Virol 80, 494–504.
Peng J, Gygi SP (2001). Proteomics: the move to mixtures. J Mass Spectrom 36, 1083–1091.
Prevostel C, Martin A, Alvaro V, Jaffiol C, Joubert D (1997). Protein kinase C alpha and tumorigenesis of the endocrine gland. Horm Res 47, 140–144.
Rapsomaniki MA, Kotsantis P, Symeonidou IE, Giakoumakis NN, Taraviras S, Lygerou Z (2012). easyFRAP: an interactive, easy-to-use tool for qualitative and quantitative analysis of FRAP data. Bioinformatics 28, 1800–1801.
Reynolds AE, Liang L, Baines JD (2004). Conformational changes in the nuclear lamina induced by herpes simplex virus type 1 require genes U(L)31 and U(L)34. J Virol 78, 5564–5575.
Scharner J, Brown CA, Bower M, Iannaccone ST, Khatri IA, Escolar D, Gordon E, Felice K, Crowe CA, Grosmann C, *et al.* (2011). Novel LMNA mutations in patients with Emery-Dreifuss muscular dystrophy and functional characterization of four LMNA mutations. Hum Mutat 32, 152–167.
Shevchenko A, Wilm M, Vorm O, Mann M (1996). Mass spectrometric sequencing of proteins silver-stained polyacrylamide gels. Anal Chem 68, 850–858.
Simon DN, Wilson KL (2013). Partners and post-translational modifications of nuclear lamins. Chromosoma 122, 13–31.
Soh JW, Weinstein IB (2003). Roles of specific isoforms of protein kinase C in the transcriptional control of cyclin D1 and related genes. J Biol Chem 278, 34709–34716.
Speese SD, Ashley J, Jokhi V, Nunnari J, Barria R, Li Y, Ataman B, Koon A, Chang YT, Li Q, *et al.* (2012). Nuclear envelope budding enables large ribonucleoprotein particle export during synaptic Wnt signaling. Cell 149, 832–846.
Stick R, Hausen P (1985). Changes in the nuclear lamina composition during early development of Xenopus laevis. Cell 41, 191–200.
Tan I, Lai J, Yong J, Li SF, Leung T (2011). Chelerythrine perturbs lamellar actomyosin filaments by selective inhibition of myotonic dystrophy kinase-related Cdc42-binding kinase. FEBS Lett 585, 1260–1268.
Urtreger AJ, Kazanietz MG, Bal de Kier Joffe ED (2012). Contribution of individual PKC isoforms to breast cancer progression. IUBMB Life 64, 18–26.
Vukovic LD, Jevtic P, Zhang Z, Stohr BA, Levy DL (2016). Nuclear size is sensitive to NTF2 protein levels in a manner dependent on Ran binding. J Cell Sci 129, 1115–1127.
Vytopil M, Benedetti S, Ricci E, Galluzzi G, Dello Russo A, Merlini L, Boriani G, Gallina M, Morandi L, Politano L, *et al.* (2003). Mutation analysis of the lamin A/C gene (LMNA) among patients with different cardiomuscular phenotypes. J Med Genet 40, e132.
Wang N, Stenkvist BG, Tribukait B (1992). Morphometry of nuclei of the normal and malignant prostate in relation to DNA ploidy. Anal Quant Cytol Histol 14, 210–216.
Wilson EB (1925). The karyoplasmic ratio. In: The Cell in Development and Heredity, New York: Macmillan, 727–733.
Zaremba-Czogalla M, Piekarowicz K, Wachowicz K, Koziol K, Dubinska-Magiera M, Rzepecki R (2012). The different function of single phosphorylation sites of Drosophila melanogaster lamin Dm and lamin C. PLoS One 7, e32649.
Zimmerman AW, Nelissen JM, van Emst-de Vries SE, Willems PH, de Lange F, Collard JG, van Leeuwen FN, Figdor CG (2004). Cytoskeletal restraints regulate homotypic ALCAM-mediated adhesion through PKCalpha independently of Rho-like GTPases. J Cell Sci 117, 2841–2852.
Zink D, Fischer AH, Nickerson JA (2004). Nuclear structure in cancer cells. Nat Rev Cancer 4, 677–687.
Zwerger M, Roschitzki-Voser H, Zbinden R, Denais C, Herrmann H, Lammerding J, Grutter MG, Medalia O (2015). Altering lamina assembly reveals lamina-dependent and -independent functions for A-type lamins. J Cell Sci 128, 3607–3620.